DESY-Bibliothek
27. OKT. 1965 ✓

DESY 65/11
September 1965
Experimente

PHOTOPRODUCTION OF PION AND NUCLEON RESONANCES AT ENERGIES UP TO 5.5 GeV

Aachen-Berlin-Bonn-Hamburg-Heidelberg-München Collaboration

U. Brall, G. Reimann,
I. Physikalisches Institut der Technischen Hochschule Aachen,

W. Bothin, H. Böttcher, K. Lanius, A. Meyer, A. Pose,
Forschungsstelle für Physik hoher Energien der Deutschen Akademie der Wissenschaften zu Berlin-Zeuthen,

J. Moebes, B. Nellen, W. Tejessy,
Physikalisches Institut der Universität Bonn und KFA Jülich, Bonn,

D. Cords, G. Harigel, G. Horlitz, E. Lohrmann, H. Meyer, M.W. Teucher, G. Wolf, DESY, Hamburg,
D. Lüke, D. Pollmann, E. Rau, P. Söding, H. Spitzer,
Physikalisches Staatsinstitut, II. Institut für Experimentalphysik, Hamburg,

H. Beisel, H. Filthuth, H. Kolar, P. Steffen,
Institut für Hochenergiephysik der Universität Heidelberg,
P. Freund, N. Schmitz, P. Seyboth, J. Seyerlein,
Max-Planck-Institut für Physik und Astrophysik, München

DEUTSCHES ELEKTRONEN-SYNCHROTRON DESY

DEUTSCHES ELEKTRONEN-SYNCHROTRON DESY, HAMBURG

Introduction

In this paper we report on photoproduction of pions and resonances by protons in the γ energy range between 0.3 GeV and 5.5 GeV. The production of N* (1238) and of the η, ρ and ω mesons has been observed. The results of ρ^0 and ω production are compared with the predictions of the one-pion-exchange (OPE) model and the diffraction model.

The experiment was carried out with the German 80-cm hydrogen bubble chamber in a Bremsstrahlung beam from the DESY electron synchrotron[1]. About 400.000 pictures were taken with an average flux of approximately 80 effective quanta per picture. The results reported here are based on about 150.000 pictures.

The flux and the energy spectrum of the incident photons were determined by counting the electron-positron pairs produced in the chamber and by measuring their energies, using the known cross sections for pair production by hydrogen.

So far we have analyzed about 5.000 events; table I gives the numbers for the different photoproduction channels. In fig. 1 the energy dependence of the cross sections for reactions (1) and (2) are shown. The curves are the corresponding values from counter and bubble chamber measurements[2]. Fig. 2 shows the cross sections for the reactions (3), (4) and (5).

Table I.

Reaction	Number	Numbers of events: Percentage of film used
(1) $\gamma p \rightarrow p\pi^{o}(\pi^{o}...)$	1465	45
(2) $n\pi^{+}(\pi^{o}...)$	1120	45
(3) $p\pi^{+}\pi^{-}$	1556	100
(4) $p\pi^{+}\pi^{-}\pi^{o}$ $(\pi^{o}...)$	691	100
(5) $n\pi^{+}\pi^{+}\pi^{-}(n^{o}...)$	280	100
(6) $p\pi^{+}\pi^{+}\pi^{-}\pi^{-}$	28	100
(7) $p\pi^{+}\pi^{+}\pi^{-}\pi^{-}\pi^{o}(\pi^{o}...)$	47	100
(8) $n\pi^{+}\pi^{+}\pi^{+}\pi^{-}\pi^{-}(\pi^{o}...)$	28	100
(9) strange particles	124	100
T o t a l	5339	

N* and ϱ^{o} production in reaction (3)

In fig. 3 and 4 we show the $p\pi^{+}$ and $\pi^{+}\pi^{-}$ mass distribution respectively from reaction (3) for different photon energy intervals. Both N^{*++} and ϱ^{o} production are obviously present. For each energy interval the two experimental mass distributions were fitted to a superposition of phase space, the Breit-Wigner distribution with an energy-dependent width[3] for the appropriate resonance and the reflection of the other resonance (assuming isotropic decay in the resonance rest frame). The sum of the three contributions as obtained from the least squares fits are shown by the curves; also the percentages for the three contri-

butions are given in the figures. From these percentages the cross sections for the two channels

$$(3a) \quad \gamma p \rightarrow N^{*++}\pi^-$$
$$(3b) \quad \gamma p \rightarrow p\,\rho^0$$

were obtained and are given as a function of the primary energy in fig. 5a and 5b. They agree with the results of the CEA bubble chamber group[4]. The cross section for N^{*++} production rises steeply from threshold up to a maximum at 0.75 GeV and then drops off rather sharply. The ρ^0 production cross section on the other hand shows the same steep rise but a much slower drop off.

In the fitting procedure discussed above the mass of the ρ-meson was used as a free parameter resulting in a best estimate of (729 ± 5) MeV. This value is lower than the commonly accepted one; however, the same tendency has been observed in other photoproduction experiments[4].

The cross section for N^{*++} production (fig. 5a) below 1.5 GeV is compatible with the prediction of Stichel and Scholz[5] who have modified the Drell formula for one-pion-exchange (OPE) to include corrections for gauge invariance. On the other hand the position and the shape of the maximum suggests that the N* is produced via the 1512 isobar (and perhaps the 1688) as an intermediate state. At energies above 1.5 GeV the comparison with the Stichel - Scholz formula is inconclusive due to the large background and the necessity for restriction to small momentum transfers.
Fig. 6 shows the distributions of the N^{*++} decay angles θ and ϕ for $E_\gamma < 1.1$ GeV and momentum transfers between incoming proton

and N^{*++} less than 0.5 GeV ^{2}. While the ϕ distribution is consistent with isotropy the cos θ distribution strongly disagrees with $(1+3\cos^2\theta)$ as predicted for OPE. Fig. 6 also gives the predictions for the OPE model with gauge invariance corrections [6]. These predictions are seen to agree with the observed distributions.

Resonance production in reaction (4)

Fig. 7 shows the $p\pi^+$ and $\pi^-\pi^0$ mass distribution for $E\gamma > 1.8$ GeV and the $\pi^+\pi^-\pi^0$ mass distribution for $E\gamma > 1.1$ GeV for reaction (4). It is seen that above 1.8 GeV there is a substantial amount of N^{*++} production corresponding to an average cross section of about 7μb. This is much larger than the amount of N^{*++} production above 2 GeV in reaction (3) (fig.5). The ρ^- is apparent in the $\pi^-\pi^0$ distribution. The accumulation of events in the mass region below 0.6 GeV is due to the pions from the decay of the ω meson (fig.7). The curve in the $\pi^-\pi^0$ distribution is a superposition of phase space and the contribution from the number of ω mesons observed above 1.8 GeV.

Fig. 5c gives the cross section for the reaction (4a) $\gamma p \to p\omega$ as a function of energy.

Production of the η meson is observed only between threshold (0.7 GeV) and 0.9 GeV; the average cross section for $\gamma p \to p\eta$ in this energy interval is $\sigma_\eta = (12.5 \pm 3.4)\mu b$. This value as well as the values of fig. 5c have been corrected for the neutral decay modes of the η (67°/o) and the ω (11°/o) respectively.

Comparison of reactions $\gamma p \to p\rho^0$ and $\gamma p \to p\omega$ with theory

At small momentum transfers the experimental cross sections for ρ^0 and ω production may be compared with the prediction of the OPE model [7] and of the diffraction model of Berman and Drell[8]. Fig.8 shows the Δ^2 distribution for reaction $\gamma p \to p\rho^0$ for primary energies up to 5.5 GeV. The shape of the distribution, as predicted by the OPE model with the form factor of Ferrari and Selleri[9], is shown by the dashed curve. It is seen that it cannot account for the steep drop off observed experimentally. This holds also for the OPE model with absorptive corrections [10] (dotted curve). The diffraction model on the other hand yields better agreement with the experimental shape (solid curve).

In fig.9 the cross sections for ρ^0 and ω production as functions of the primary energy are shown for $\Delta^2 < 0{,}5$ GeV^2. For ρ^0 production the OPE model predicts a rather steep fall-off with increasing energy whereas the experimental cross section seems to be rather constant. On the other hand such a behaviour is expected from the diffraction model.

We now use the OPE and the diffraction model to make quantitative estimates for the partial widths $\Gamma_{\rho\pi\gamma}$ and $\Gamma_{\omega\pi\gamma}$ for the decays $\rho \to \pi\gamma$ and $\omega \to \pi\gamma$ respectively. The contribution of the OPE model to $\rho^0(\omega)$ production is proportional to $\Gamma_{\rho\pi\gamma}$ ($\Gamma_{\omega\pi\gamma}$). On the other hand the diffraction model yields a contribution proportional to $\Gamma_{\omega\pi\gamma} \cdot \frac{g^2_{\omega\rho\pi}}{4\pi} / \Gamma^2_{\rho\pi\pi}$ for ρ^0 production and proportional to $\Gamma_{\rho\pi\gamma} \cdot \frac{g^2_{\omega\rho\pi}}{4\pi} / \Gamma^2_{\rho\pi\pi}$ for ω production. In these expressions $\Gamma_{\rho\pi\pi}$ is the width for the decay $\rho \to 2\pi$ and $g_{\omega\rho\pi}$ the $\omega\rho\pi$ coupling constant. In the following

the values $\overline{\Gamma}_{\rho\pi\pi}$ = 140 MeV and $\frac{g^2_{\omega\rho\pi}}{4\pi}$ = 12 [8a] were used . Fo
ω production the OPE model leads to reasonable agreement with the experimental cross sections if one uses a value of $\overline{\Gamma}_{\omega\pi\gamma} \simeq 0.7$ MeV (fig. 9b, dashed curve). This number may be compared with 0.9MeV as obtained from direct observation of the decay mode $\omega \to \pi\gamma$ [11]. Applying the diffraction model one has to take $\overline{\Gamma}_{\rho\pi\gamma}$ as small as 0.1 MeV in order to find agreement with the experimental results (solid curve).

With these values for $\overline{\Gamma}_{\omega\pi\gamma}$ and $\overline{\Gamma}_{\rho\pi\gamma}$ one can now calculate the contributions of the OPE model and the diffraction model to ρ^0 production (fig.9a, dashed and solid curve respectively). The contribution from OPE is negligible in accordance with the observations discussed above whereas the diffraction model agrees roughly with the experimental values.

The value obtained for the ratio $\frac{\overline{\Gamma}_{\omega\pi\gamma}}{\overline{\Gamma}_{\rho\pi\gamma}}$ is compatible with the prediction 9:1 from SU(6) [12].

A c k n o w l e d g e m e n t s:

We are greatly indebted to the machine group of DESY for all their efforts and for the excellent performance of the synchrotron, and to the operating crews of the bubble chamber, the hydrogen liquifier, and the beam line. We also thank our scanners for their painstaking work. The work in the laboratories in Aachen, Bonn, Hamburg (II. Institut für Experimentalphysik), Heidelberg and München was supported by the Bundesministerium für Wissenschaftliche Forschung.

Appendix

N^*_{33} production in the reaction $\gamma p \to N^{*++}_{33} \pi^-$

The N^*_{33} decay angular distribution may be expressed by

$$W(\cos\Theta, \Phi) = \frac{3}{4\pi}\left\{\frac{1}{6}\rho_{11} + \frac{1}{2}\rho_{33} + \frac{1}{2}(\rho_{11} - \rho_{33})\cos^2\Theta - \frac{1}{\sqrt{3}}\mathrm{Re}\,\rho_{31}\sin 2\Theta\cos\phi - \frac{1}{\sqrt{3}}\mathrm{Re}\,\rho_{3-1}\sin^2\Theta\cos 2\phi\right\}$$

Θ is the angle between incident and outgoing proton and ϕ the azimuth angle ($\phi = 0$ in the production plane), both taken in the N^* rest frame. In the model of Stichel and Scholz the density matrix elements ρ_{ij} are given by[6]

$$\rho_{11} = C\left\{\frac{8}{3}\frac{\mu^2}{(t-\mu^2)^2}[P_1P_1] + \frac{1}{6}g_1(s,t)\cdot\left([qq] + 3\frac{[P_1q]^2}{[P_1P_1]}\right) - 1 - \frac{4}{3}g_2(s,t)[qP_1]\right\}$$

$$\rho_{3-1} = -C\left\{\frac{1}{2\sqrt{3}}g_1(s,t)\cdot\left([kk] - \frac{[P_1k]^2}{[P_1P_1]}\right)\right\}$$

$$\rho_{31} = C\left\{\frac{-1}{\sqrt{3}}g_1(s,t)\frac{[qP_1]}{[P_1P_1]}\cdot\left([P_1P_1][qq] - [qP_1]^2\right)^{1/2} + \frac{1}{\sqrt{3}}g_2(s,t)\cdot\left([P_1P_1][qq] - [qP_1]^2\right)^{1/2}\right\}$$

$$\rho_{33} = C\left\{\frac{1}{2}g_1(s,t)\cdot\left([kk] - \frac{[P_1k]^2}{[P_1P_1]}\right) - 1\right\}$$

with

$$g_1(s,t) = \left(\frac{1}{2} \frac{P_1}{s-m^2} + \frac{5}{2} \frac{P_2}{u-M^2} \right)^2$$

$$g_2(s,t) = \frac{P_1 q}{(s-m^2)(t-\mu^2)} + \frac{5 P_2 q}{(t-\mu^2)(u-M^2)} + \frac{2}{t-\mu^2} - \frac{1}{2(s-m^2)}$$

$$C = \frac{1}{\varrho_{11} + \varrho_{33}}$$

Here k, p_1; q, p_2 denote the fourmomenta of the photon, of the incident proton, of the π^- and of the isobar respectively.
μ is the pion mass, m is the nucleon mass and M is the isobar mass;

$$s = (k + p_1)^2$$
$$t = (k - q)^2$$
$$u = (p_1 - q)^2$$
$$[a\ b] = \vec{a} \cdot \vec{b}$$

$\vec{a}, \vec{b}$ are the three momenta of a,b in the isobar rest frame.

References

1) Aachen-Berlin-Bonn-Hamburg-Heidelberg-München Collaboration, Proceedings of the International Symposium on Electron and Photon Interactions at High Energies, Hamburg (1965), to be published

2) see Ph. Salin, Nuovo Cimento 28, 1294 (1963)

G. Ascoli, E.L. Goldwasser, U.E. Kruse, J. Simpson, W.P. Swanson, Proceedings of the Sienna International Conference on Elementary Particles, Vol. I, 485 (1963);

R.L. Walker, Proceedings of the Conference on Photon Interactions in the BeV-Energy Range, Cambridge, Vol. IV, 1 (1963);

D.A. Mc Pherson, D.C. Gates, R.W. Kenney, W.P. Swanson, Physical Review 136, B 1465 (1964)

3) J.D. Jackson, Nuovo Cimento 34, 1644 (1964)

4) Cambridge Bubble Chamber Group, Proceedings of the International Symposium on Electron and Photon Interactions at High Energies, Hamburg (1965), to be published

B. Elsner, H. Blechschmidt, K. Heinloth, A. Ladage, J. Rathje, and D. Schmidt, Proceedings of the International Symposium on Electron and Photon Interactions at High Energies, Hamburg (1965), to be published

L.J. Lanzerotti, R.B. Blumenthal, D.C. Ehn, W.L. Faissler, P.M. Joseph, F.M. Pipkin, J.K. Randolph, J.J. Russell, D.G. Stairs and J. Tenenbaum, Physical Review Letters 15, 210 (1965)

5) P. Stichel and M. Scholz, Nuovo Cimento 34, 1381 (1964)

6) M. Scheunert and P. Stichel, private communication

7) H. Joos and G. Kramer, Zeitschrift für Physik 178, 542 (1964)

8) S.M. Berman and S.D. Drell, Phys. Review 133, B 791 (1964)

9) E. Ferrari and F. Selleri, Nuovo Cimento 27, 1450 (1963)

10) J.D. Jackson, private communication;

K. Schilling, International Symposium on Electron and Photon Interactions at High Energies, Hamburg (1965), to be published

11) A.H. Rosenfeld, A. Barbaro-Galtieri, W.H. Barkas, P.L. Bastien, J. Kirz and M. Roos, UCRL - 8030 Part I, March 1965

12) S. Badier and C. Bouchiat, ORSAY preprint (1965).
W. E. Thirring, VIENNA preprint.

8a) R.F. Dashen and D.H. Sharp, Phys. Review 133, B1585 (1964)

Captions for figures

Fig. 1 Cross sections for (a) $\gamma p \to p\pi^0$ and (b) $\gamma p \to n\pi^+$ as functions of the photon energy E_γ. E_γ was calculated under the assumption that only one pion is produced. The curves show the cross sections from counter and bubble chamber measurements (ref.2).

Fig. 2 Cross sections for (a) $\gamma p \to p\pi^+\pi^-$ and (b) $\gamma p \to \pi^+\pi^-\pi^0$(•) and $\gamma p \to n\pi^+\pi^+\pi^-$(Δ) as functions of the photon energy.

Fig. 3 $p\pi^+$ effective mass distributions for reaction $\gamma p \to p\pi^+\pi^-$ for different energy intervals of the incident photons. The curves are superpositions of phase space (P.S.), a Breit-Wigner distribution for N^{*++} and the reflection from the ϱ^0 meson, obtained from a least squares fit.

Fig. 4 $\pi^+\pi^-$ effective mass distributions for reaction $\gamma p \to p\pi^+\pi^-$ for different energy intervals of the incident photons. The curves are superpositions of phase space (P.S.), a Breit-Wigner distribution for the ϱ^0 meson and the reflection from the N^{*++}, obtained from a least squares fit.

Fig. 5 Cross sections for (a) $\gamma p \to N^{*++}\pi^-$, (b) $\gamma p \to p\varrho^0$ and (c) $\gamma p \to p\omega$ as functions of the photon energy.

Fig. 6 Distributions of the N^{*++} decay angles θ and ϕ for $E_\gamma < 1.1$ GeV, $\Delta^2(p/p\pi^+) < 0.5$ GeV^2 and $1.12\ \text{GeV} < M_{p\pi^+} < 1.32$ GeV for reaction $\gamma p \to p\pi^+\pi^-$. θ is the angle between incident and outgoing proton and ϕ the azimuth angle ($\phi = 0$ in the production plane), both taken in the N^{*++} rest frame. The curves give the predictions of the OPE model, and of the OPE model with the corrections of Stichel and Scholz.

Fig. 7 Effective mass distributions of (a) $p\pi^+$ and (b) $\pi^-\pi^0$ for $E_\gamma > 1.8$ GeV and of (c) $\pi^+\pi^-\pi^0$ for $E_\gamma > 1.1$ GeV for reaction $\gamma p \to p\pi^+\pi^-\pi^0$. The curve in (a) is the phase space distribution, the curve in (b) is a superposition of phase space and the reflection from ω decay.

Fig. 8 $\frac{d\sigma}{d\Delta^2}$ for reaction $\gamma p \to p\rho^0$ for $E_\gamma < 5.5$ GeV. The dashed curve is the prediction of the OPE model with the Ferrari-Selleri form factor, the dotted one of OPE with corrections for absorption. The solid curve is the prediction of the diffraction model with $\Gamma_{\omega\pi\gamma} = 0.7$ MeV, $\Gamma_{\rho\pi\pi} = 140$ MeV and $\frac{g^2_{\omega\rho\pi}}{4\pi} = 12$ (see text).

Fig. 9 Cross sections for (a) $\gamma p \to p\rho^0$ and (b) $\gamma P \to p\omega$ as functions of photon energy for $\Delta^2(p/p) < 0.5$ GeV^2. The solid and dashed curves show the predictions of the diffraction and the OPE model with the Ferrari Selleri form factor. The values $\Gamma_{\omega\pi\gamma} = 0.7$ MeV, $\Gamma_{\rho\pi\gamma} = 0.1$ MeV, $\Gamma_{\rho\pi\pi} = 140$ MeV and $\frac{g^2_{\omega\rho\pi}}{4\pi} = 12$ were used (see text).

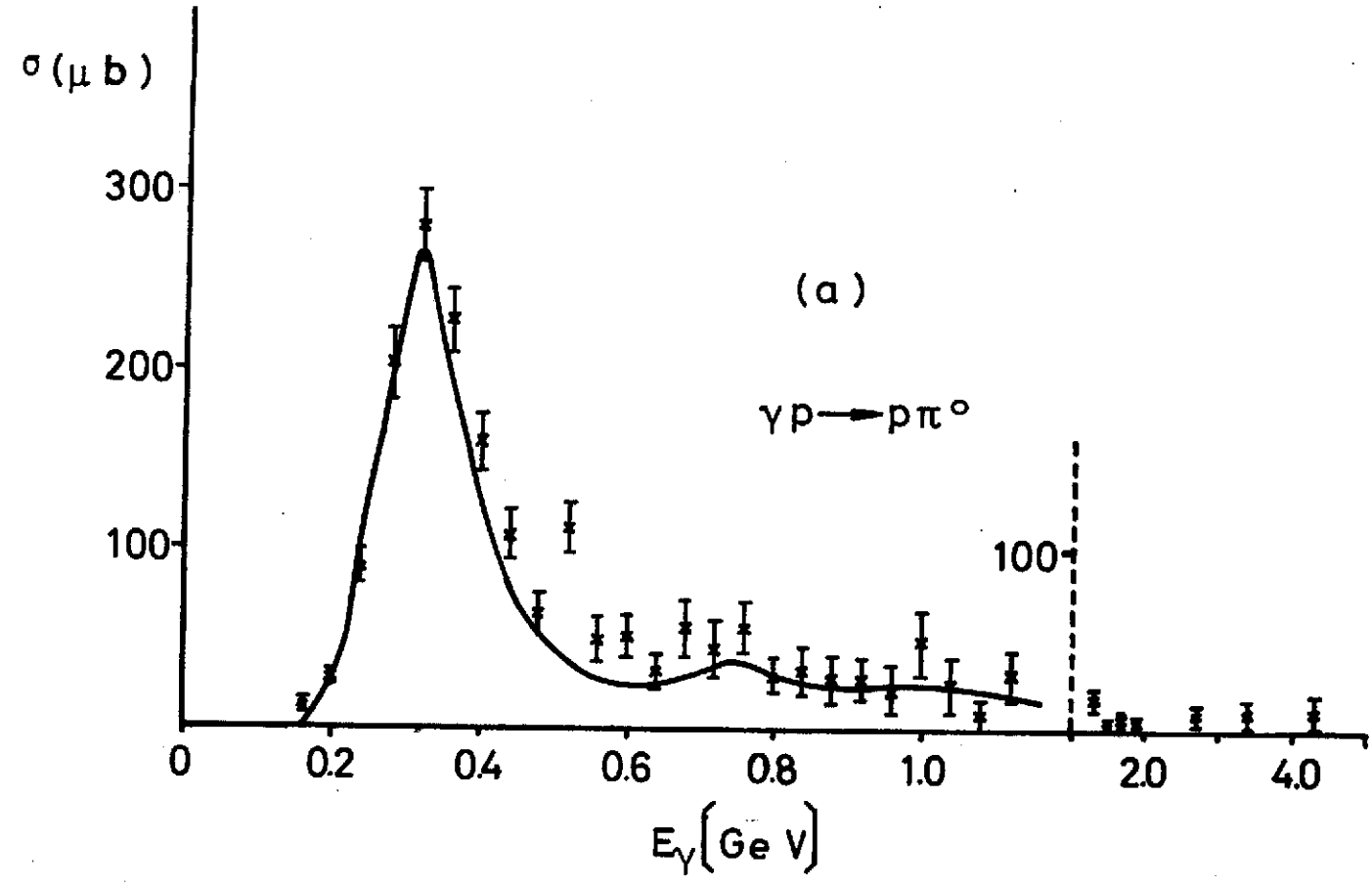
σ (μ b)
300
200
100
(a)
γp → pπ°
100
0
0.2
0.4
0.6
0.8
1.0
2.0
4.0
Eγ (Ge V)

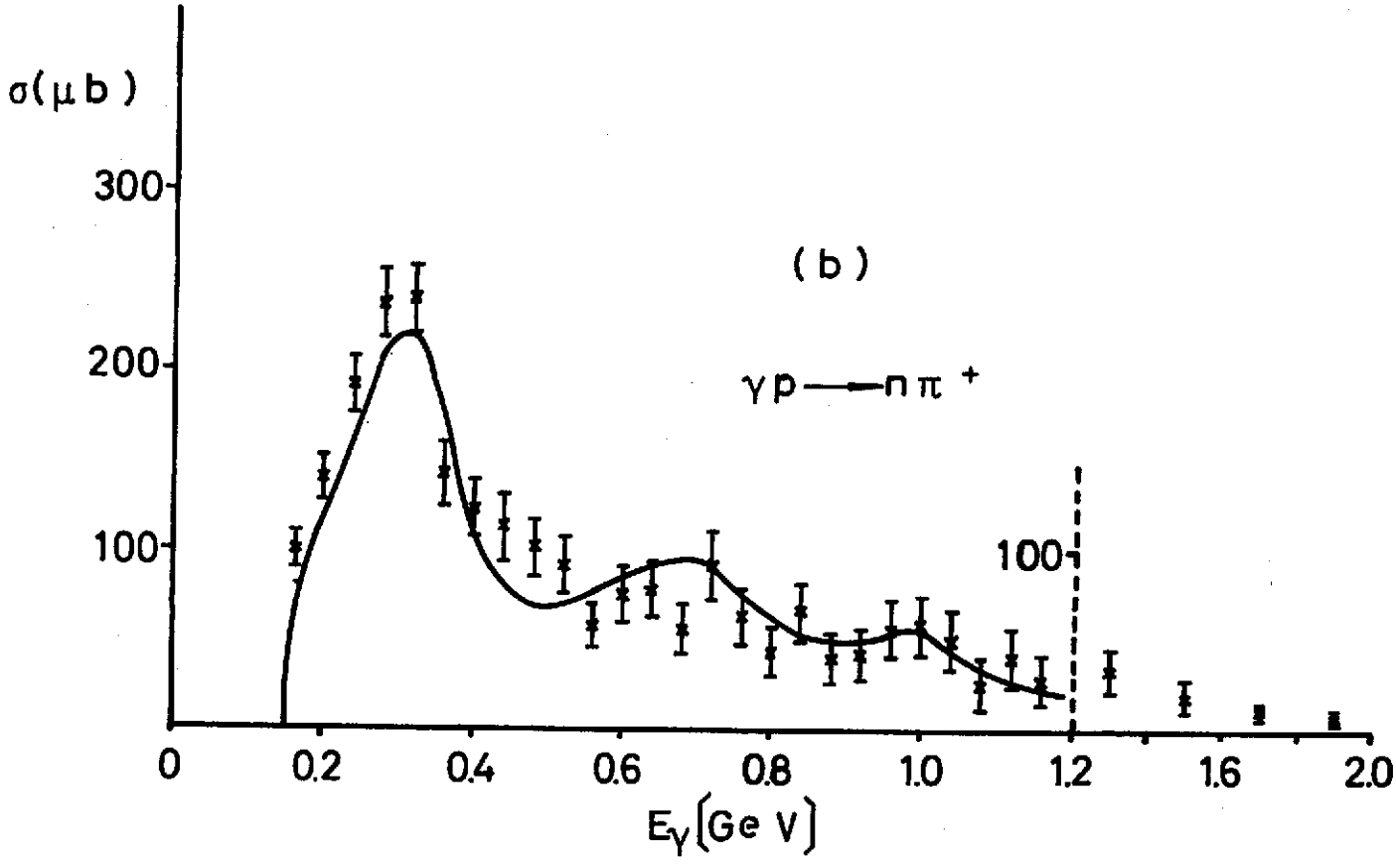
σ(μb)
300
200
100
(b)
γp → nπ+
100
0
0.2
0.4
0.6
0.8
1.0
1.2
1.6
2.0
Eγ (Ge V)

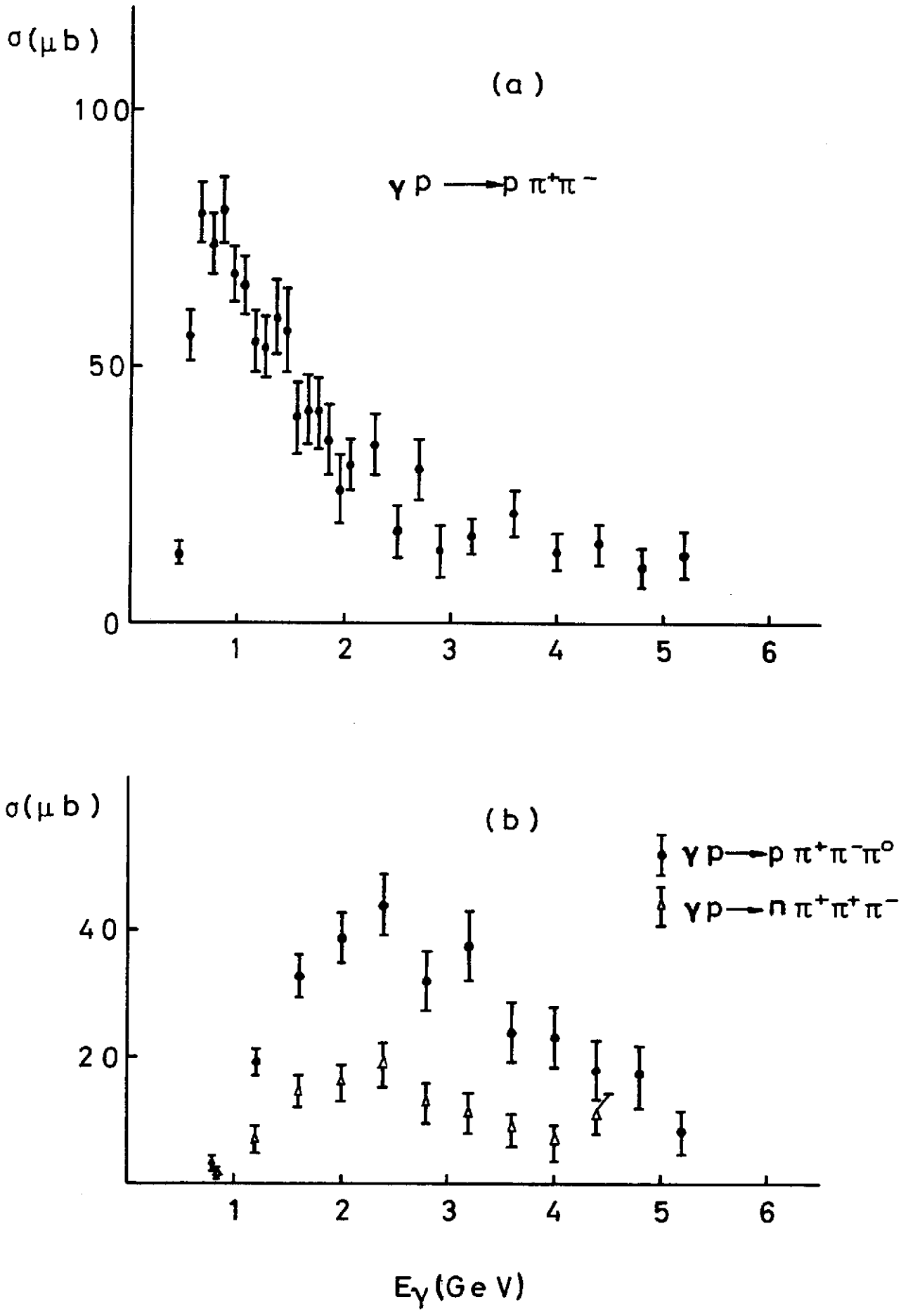
σ(μb)
(a)
100
50
0
γp → pπ⁺π⁻
1
2
3
4
5
6
σ(μb)
(b)
40
20
γp → pπ⁺π⁻π°
γp → nπ⁺π⁺π⁻
1
2
3
4
5
6
Eγ (GeV)

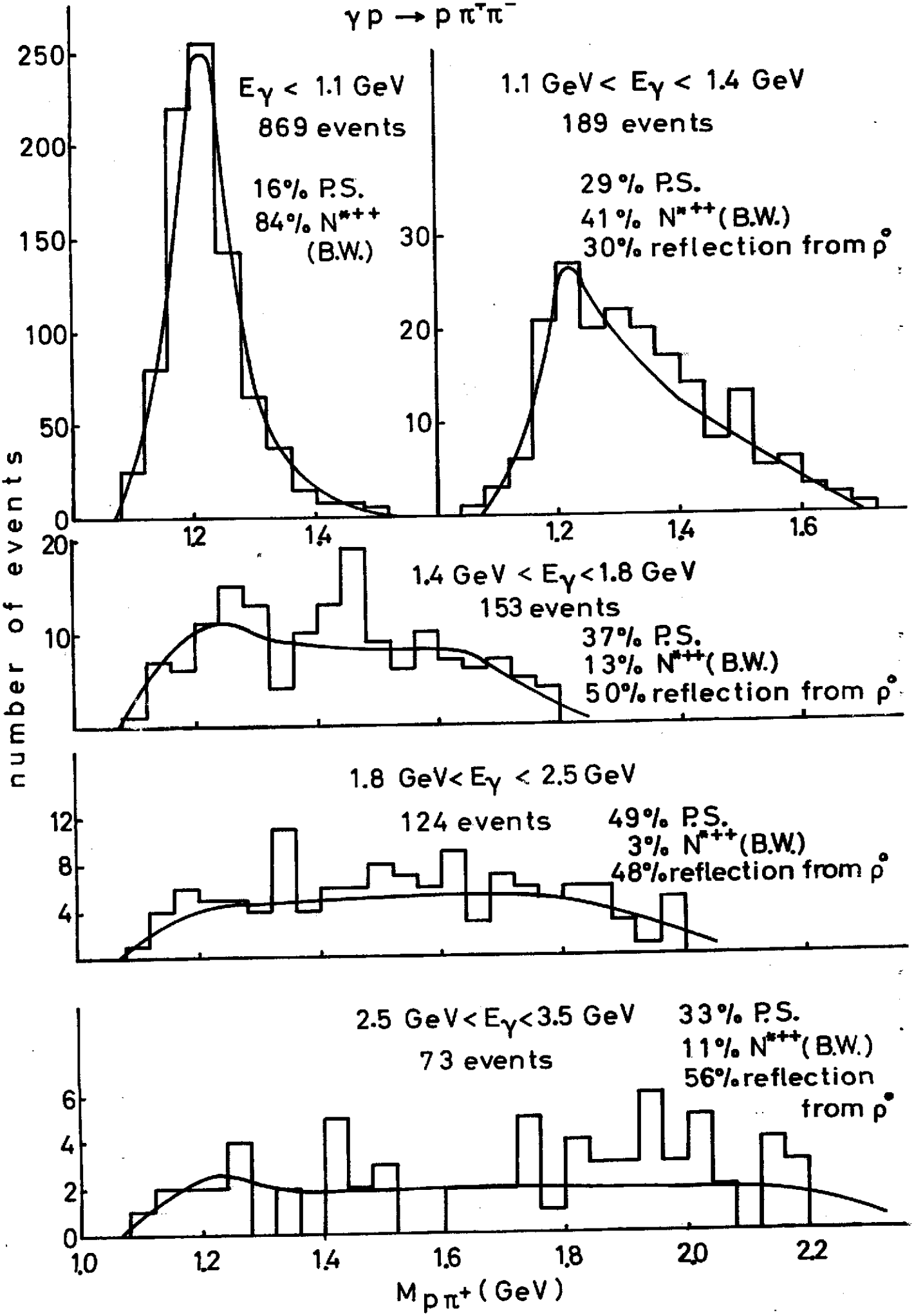
γ p → p π⁺π⁻
Eγ < 1.1 GeV
869 events
16% P.S.
84% N*++ (B.W.)
1.1 GeV < Eγ < 1.4 GeV
189 events
29% P.S.
41% N*++ (B.W.)
30% reflection from ρ°
1.4 GeV < Eγ < 1.8 GeV
153 events
37% P.S.
13% N*++ (B.W.)
50% reflection from ρ°
1.8 GeV < Eγ < 2.5 GeV
124 events
49% P.S.
3% N*++ (B.W.)
48% reflection from ρ°
2.5 GeV < Eγ < 3.5 GeV
73 events
33% P.S.
11% N*++ (B.W.)
56% reflection from ρ°
number of events
M p π⁺ (GeV)

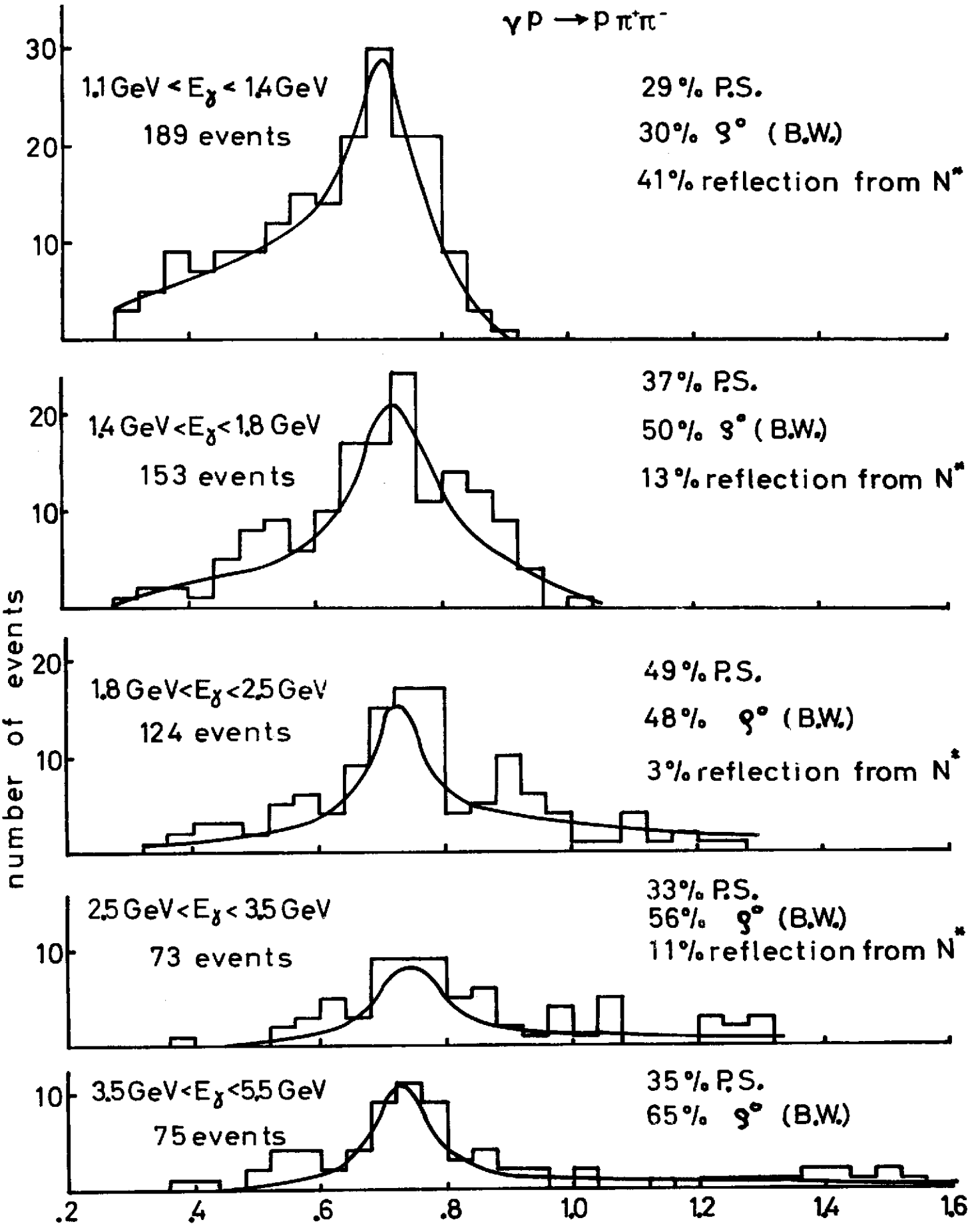
γp → pπ⁺π⁻
1.1 GeV < Eγ < 1.4 GeV
189 events
29% P.S.
30% ρ° (B.W.)
41% reflection from N*
1.4 GeV < Eγ < 1.8 GeV
153 events
37% P.S.
50% ρ° (B.W.)
13% reflection from N*
1.8 GeV < Eγ < 2.5 GeV
124 events
49% P.S.
48% ρ° (B.W.)
3% reflection from N*
2.5 GeV < Eγ < 3.5 GeV
73 events
33% P.S.
56% ρ° (B.W.)
11% reflection from N*
3.5 GeV < Eγ < 5.5 GeV
75 events
35% P.S.
65% ρ° (B.W.)
number of events
Mπ⁺π⁻ (GeV)

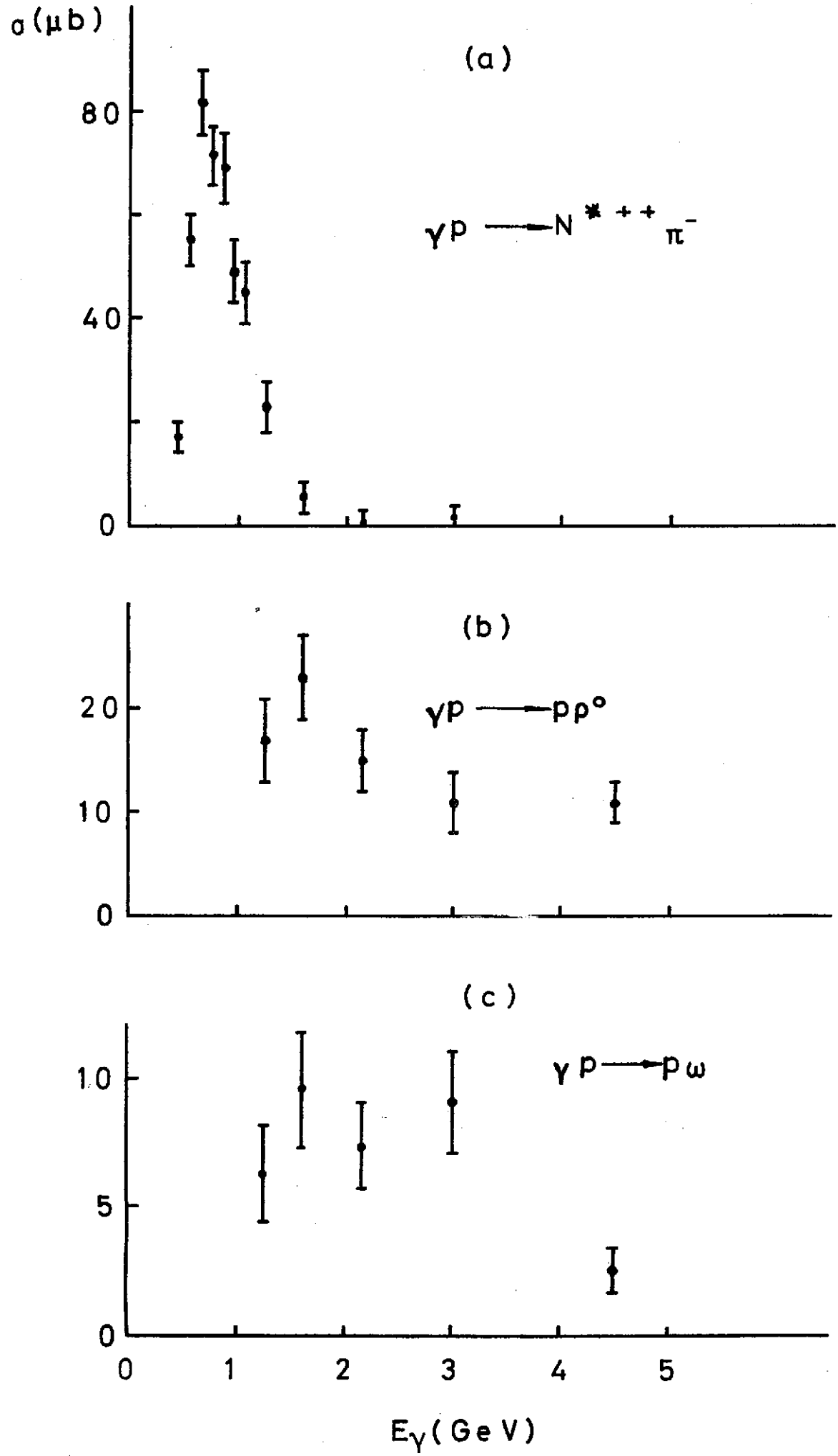
σ(μb)
(a)
80
40
0
γp ⟶ N* ++ π⁻
(b)
20
10
0
γp ⟶ pρ°
(c)
10
5
0
γp ⟶ pω
0
1
2
3
4
5
Eγ(GeV)

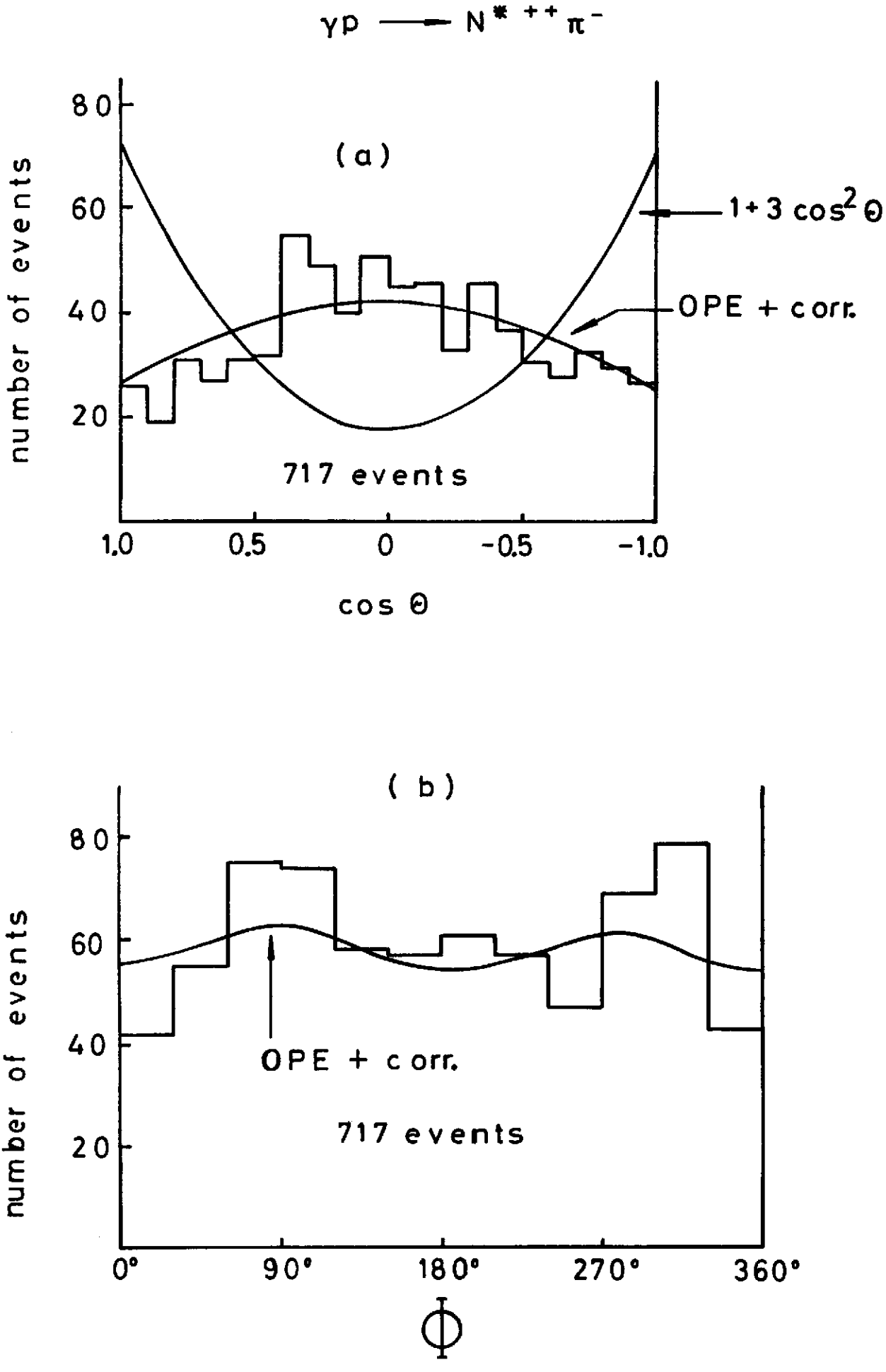
γp → N* ++ π-
(a)
number of events
80
60
40
20
1+3 cos²Θ
OPE + corr.
717 events
1.0
0.5
0
-0.5
-1.0
cos Θ
(b)
number of events
80
60
40
20
OPE + corr.
717 events
0°
90°
180°
270°
360°
Φ

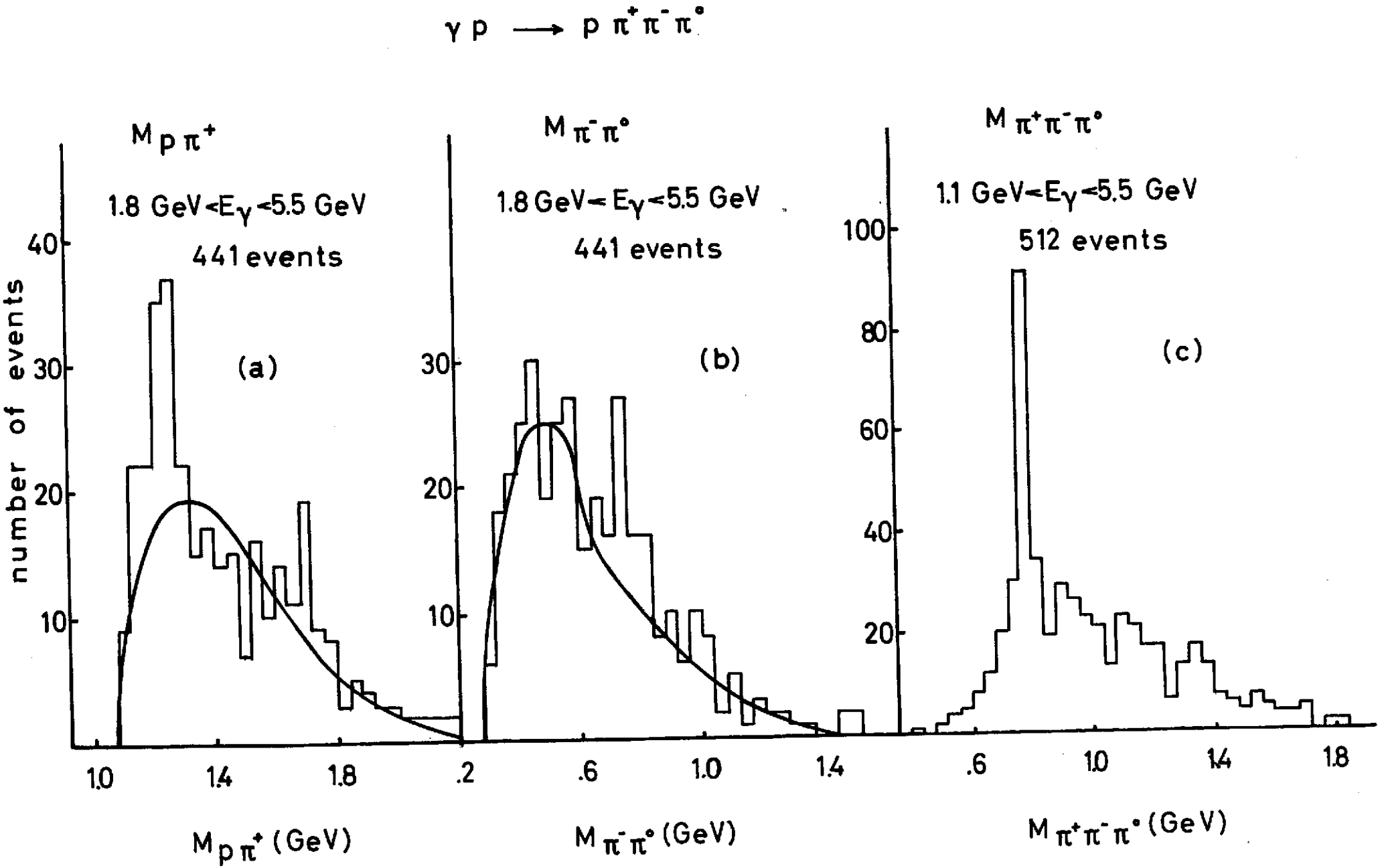
γ p ⟶ p π⁺ π⁻ π°
M p π⁺
1.8 GeV<Eγ<5.5 GeV
441 events
(a)
M π⁻ π°
1.8 GeV< Eγ<5.5 GeV
441 events
(b)
M π⁺ π⁻ π°
1.1 GeV<Eγ<5.5 GeV
512 events
(c)
number of events
M p π⁺ (GeV)
M π⁻ π° (GeV)
M π⁺ π⁻ π° (GeV)

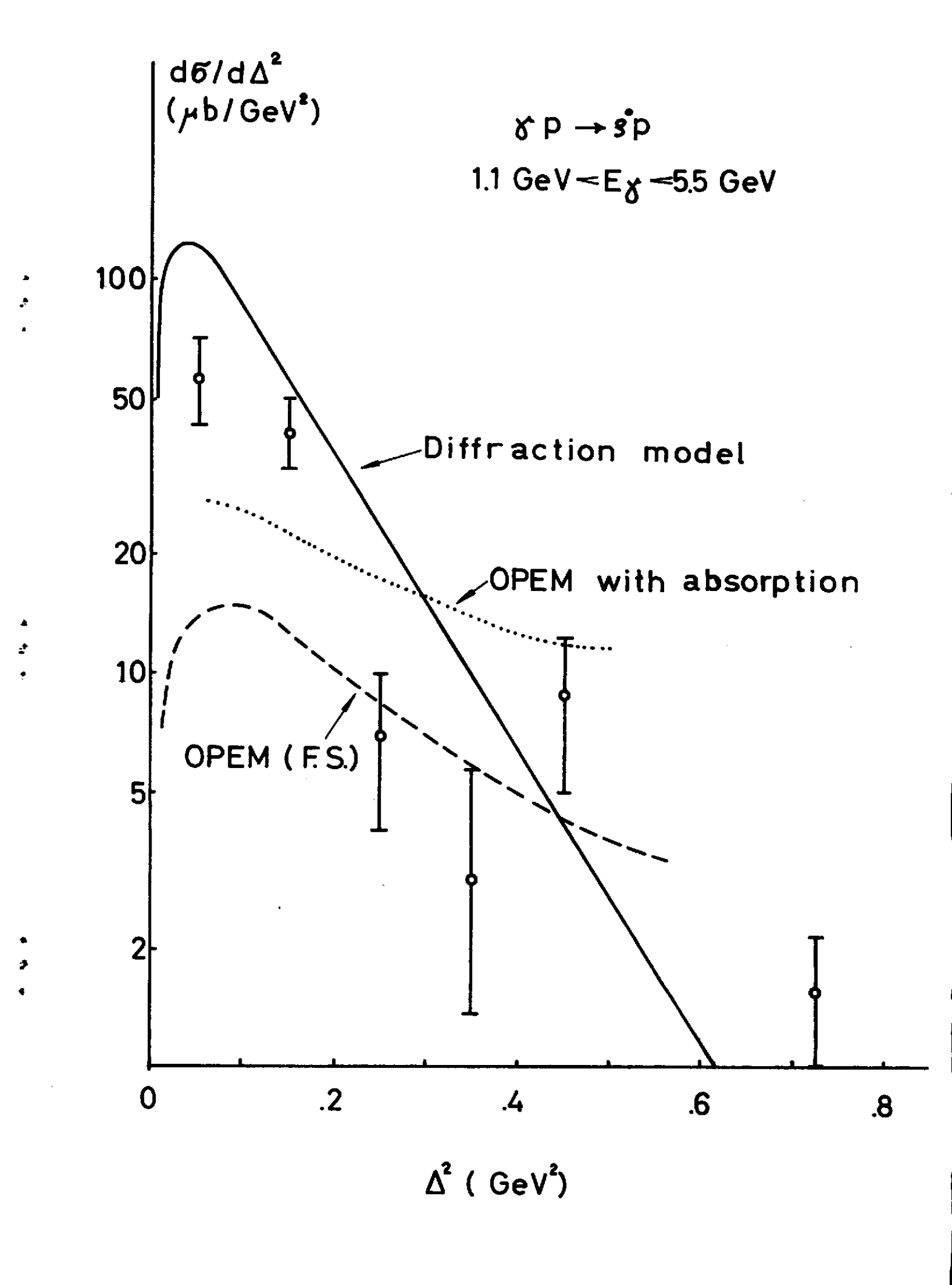
dσ/dΔ²
(μb/GeV²)
γ p → s° p
1.1 GeV < Eγ < 5.5 GeV
100
50
20
10
5
2
Diffraction model
OPEM with absorption
OPEM (F.S.)
0
.2
.4
.6
.8
Δ² (GeV²)

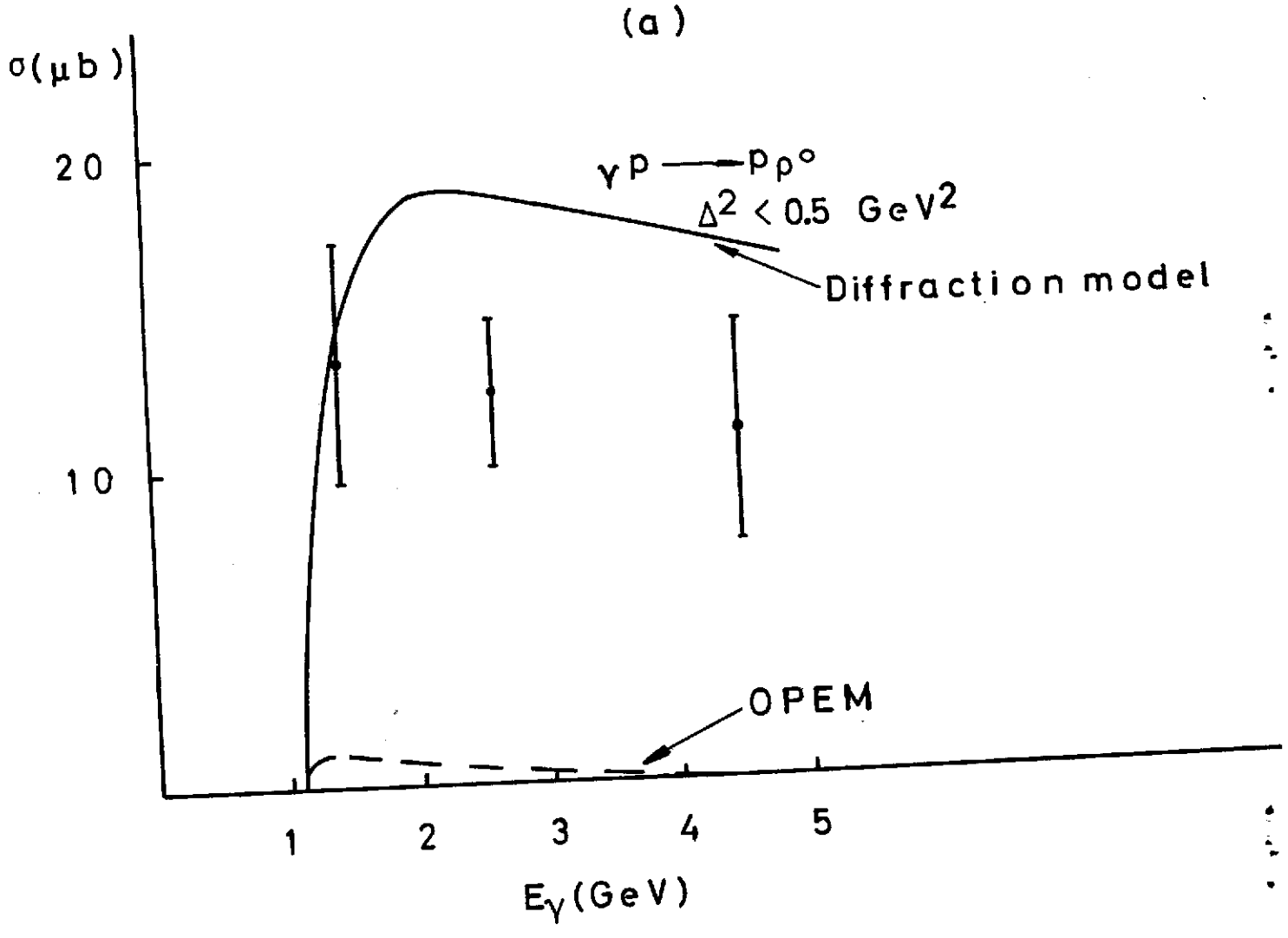
(a)
σ(μb)
20
10
γp → pρ°
Δ² < 0.5 GeV²
Diffraction model
OPEM
1
2
3
4
5
Eγ(GeV)

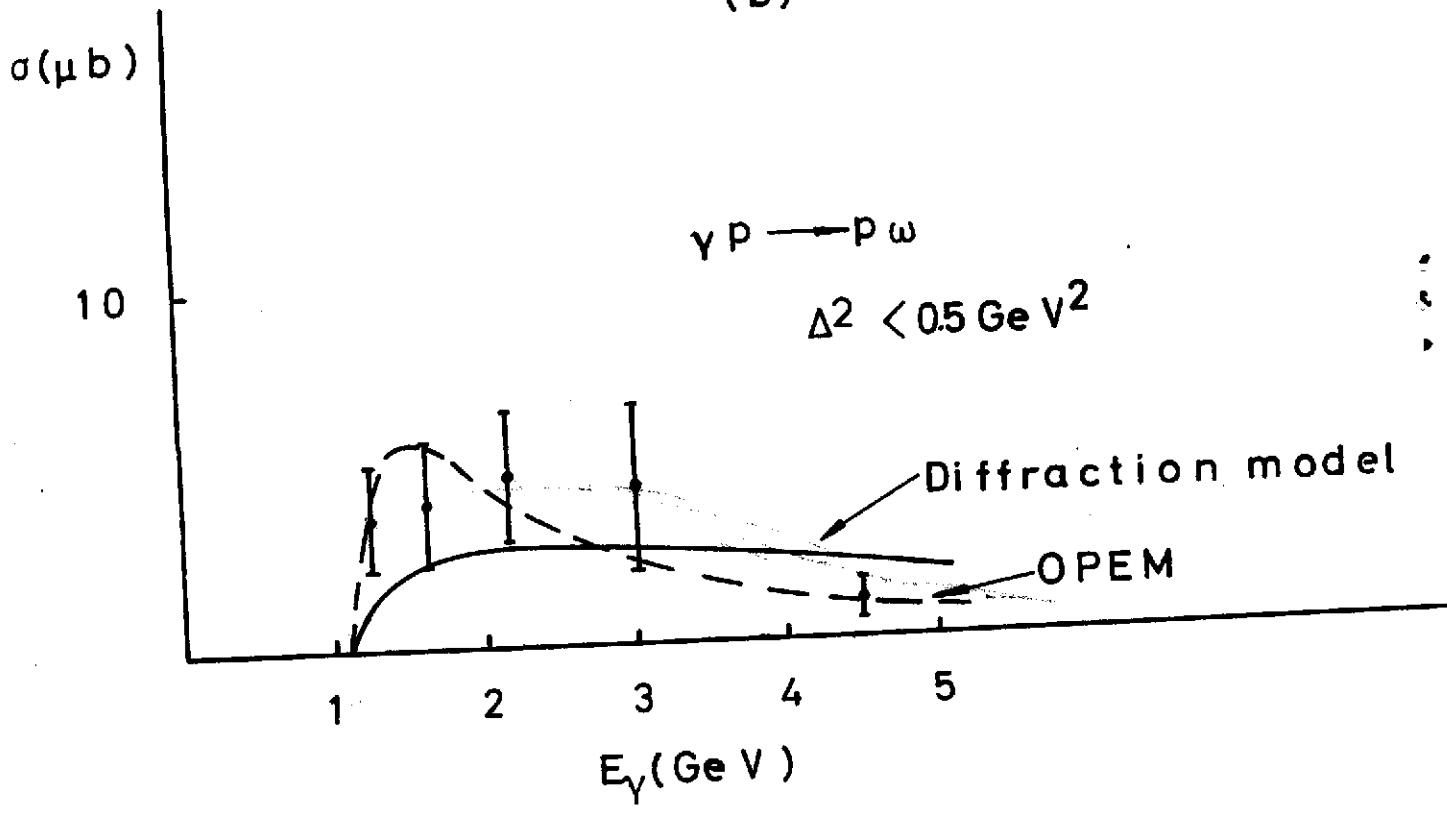
(b)
σ(μb)
10
γp → pω
Δ² < 0.5 GeV²
Diffraction model
OPEM
1
2
3
4
5
Eγ(GeV)